Tanzania Journal of Science 46(3): 661-672, 2020
ISSN 0856-1761, e-ISSN 2507-7961
© College of Natural and Applied Sciences, University of Dar es Salaam, 2020

Synthesis and FTIR Characterization of Mg-Hydroxylapatite Derived from Dolostone with High Dolomite Mineral Content

Wilson L. Mahene[1*], Charles Gervas[2], Askwar H Hilonga[1] and Revocatus L Machunda[1]
[1]*Department of Materials, Energy Science and Engineering, the Nelson Mandela African Institution of Science and Technology, P. O. Box 447 Arusha, Tanzania.*
[2]*St. Augustine University of Tanzania Arusha, P. O. Box 12385 Arusha, Tanzania*
**Corresponding author: wilson.mahene@nm-aist.ac.tz*
Co-authors emails: rufcharles@gmail.com, askwar.hilonga@nm-aist.ac.tz, revocatus.machunda@nm-aist.ac.tz
Received 8 July 2020, Revised 23 Aug 2020, Accepted 24 Aug 2020, Published Oct 2020
https://dx.doi.org/10.4314/tjs.v46i3.8

Abstract

We present the synthesis of magnesium-substituted hydroxylapatite starting from locally available dolostone. The apatite was prepared by a reaction between heat pre-treated dolostone powder with phosphoric acid, maintained at the pH of 12.5 using sodium hydroxide. The resultant material was then calcined at 500 °C, 600 °C, 700 °C, 800 °C and 900 °C. The precursor dolostone was characterized by organic elemental analyser (CHNS-O analyser), X-ray fluorescence (XRF) and Fourier transform infrared spectroscopy (FTIR), while the synthesized material was characterized by using FTIR. Results indicated that the dominant mineral in the carbonate rock materials was near-stoichiometric dolomite, while the synthesized material was found to be (carbonate, magnesium)-substituted hydroxylapatite. The synthesized material did not exhibit hydroxylapatite diagnostic peaks until after being calcined at 600 °C. The peaks became more distinct with increase in calcination temperature. The prepared material exhibited a low degree of crystallinity and low conversion temperature to beta-tricalcium phosphate, 700–800 °C. These characteristics are typical of a magnesium-substituted hydroxylapatite (Mg-substituted β-tricalcium phosphate). This work has demonstrated the feasibility of synthesizing magnesium-substituted hydroxylapatite (Mg-HA), with potential applications in water purification, using dolostone as a calcium/magnesium source.

Keywords: Dolostone, crystallinity, magnesium-substituted hydroxylapatite, magnesium-substituted beta-tricalcium phosphate.

Introduction

Hydroxylapatite (HA), $Ca_5(PO_4)_3(OH)$ (pentacalcium hydroxide triphosphate) (also $Ca_{10}(PO_4)_6(OH)_2$), is an isomorph of naturally occurring fluorapatite, $Ca_{10}(PO_4)_6F_2$. It is the principal inorganic constituent of human bones and teeth, and consequently has become a topic of extensive biological and physico-chemical investigations. Owing to its biocompatibility, HA finds applications in bone reconstruction and repair surgery, dental implantology, and pharmacy. This compound is known to be capable of undergoing ion-exchange when it is in aqueous solution. The hydroxyl ions may be replaced by ions of similar size and charge, such as Cl^- or F^-. Calcium ions may also be substituted by ions such as Mg^{2+}, Mn^{2+}, or Sr^{2+} (Kolmas et al. 2014). There is also a possibility that the ions involved in the substitution are of different

charges. For instance, a phosphate ion (−3) may be replaced by a carbonate ion (−2), forming a positively charged vacancy. The positive charge necessitates a simultaneous release of one cation of calcium (Ca^{2+}) and one hydroxyl ion (OH^-) to re-establish neutrality (Kolmas et al. 2014). The ability of hydroxylapatite to exchange ions with its aqueous environment is used in water purification to remove ionic contaminants from water such as fluoride and heavy metals (Avram et al. 2017, Mousa et al. 2016). It also presents the possibility to incorporate antibacterial ions such as silver, copper and zinc, in its lattice to slowly release them into water for their desired actions. Hydroxylapatite also removes fluoride from water by electrostatic adsorption and precipitation (Sternitzke et al. 2012).

Natural hydroxylapatite from animal bones is currently used in the developing world for water purification; fluoride and heavy metal removal from drinking water (Wagutu et al. 2018). The use of natural bones, however, is facing regeneration challenges and it is not universally accepted on cultural grounds (Wagutu et al. 2018). Due to the drawbacks, research is now turning to synthetic hydroxylapatite for fluoride removal (Wagutu et al. 2018) and heavy metal removal from water (Avram et al. 2017, Mousa et al. 2016).

This mineral (HA) can be synthesized by precipitation using phosphoric acid (or phosphate salt) and calcium in a basic medium (Narasaraju and Phebe 1996). To synthesize hydroxylapatite, various calcium sources, such as eggshells, crustacean shells (Wagutu et al. 2018), corals (Xu et al. 2001), carbonate rocks (Jamarun et al. 2015, Klinkaewnarong and Utara 2018), commercial analytical grade calcium hydroxide and calcium oxide have been used. The use of limestone (calcite) as a source of calcium has been extensively studied in the synthesis of hydroxylapatite (Jamarun et al. 2015, Klinkaewnarong and Utara 2018). However, despite its abundance on the earth's crust, limited studies have used dolostone to synthesize hydroxylapatite. The use of dolomite in the synthesis of HA is interesting as it may form magnesium-substituted hydroxylapatite (Mg-HA) which has been reported to have antimicrobial properties due to the presence of magnesium (Alioui et al. 2019, Demishtein et al. 2019, Predoi et al. 2019, Suphatchaya et al. 2019). The authors therefore expect that, in addition to removal of heavy metals and fluoride, the dolomite-derived hydroxylapatite will also disinfect water and prevent the apatite material from the risk of harboruring microbes. Magnesium-substituted hydroxylapatite can also be prepared by including magnesium ions in the reacting mixture (Bertoni et al. 1998). It is common knowledge that dolomite decomposes upon heating at high tempeature (above 950 °C) to magnesium oxide and calcium oxide according to Equation 1.

$$CaMg(CO_3)_2 \xrightarrow{\Delta} CaO + MgO + 2CO_2 \quad (1)$$

The oxides form their respective hydroxides upon contact with water. The hydroxides react with phosphoric acid under high pH to form Mg-HA according to Equation 2.

$$10\text{-}xCa(OH)_2 + xMg(OH)_2 + 6H_3PO_4 \rightarrow Ca_{10-x}Mg_x(PO_4)_6(OH)_2 + 18H_2O \quad (2)$$

The actual reaction could be far more complicated as the formed hydroxylapatite may contain unoccupied sites in its structure due to ionic substitutions (Kolmas et al. 2014) leading to non-stochiometric reaction and composition.

This work aimed to investigate the feasibility of using heat pre-treated locally available dolostone to synthesize magnesium-substituted hydroxylapatite (Mg-HA) with potential applications in water purification; water de-fluoridation, heavy metal removal and disinfection. Therefore, in this paper, we report a novel and potentially an industrially applicable method to synthesize Mg-HA using readily available dolomite as a calcium/magnesium source.

Materials and Methods

Material collection

Dolostones were collected from Kwamsisi village, in Kwamsisi ward Korogwe district in Tanga region, Tanzania, in April 2019. The rocks were mined using handpicks and hammer at a dolomite mine site where local people mine the rocks for construction and decoration. Reagent grade phosphoric acid was obtained from Sigma Aldrich.

Material preparation

The dolostones were reduced in size with a steel hummer and ground in a ceramic ball mill at the African Minerals and Geosciences Centre in Dar-es-Salaam, Tanzania. The powder was sieved through a 212 μm sieve. The obtained powder was heat pre-treated at 970 °C for 8 hours decomposing it into calcium oxide and magnesium oxide according to Equation 1.

Mg-hydroxylapatite synthesis

The magnesium-substituted hydroxylapatite (Mg-HA) was synthesized by a reaction of the heat pretreated dolostone powder with phosphoric acid maintained at a pH of 12.5 ± 0.5 using sodium hydroxide solution. Exactly 20.0 g of the powder was mixed with 400 mL of distilled water in a 1 L glass beaker and stirred with a glass rod. The mixture became hot due to the reaction of the oxides (CaO and MgO) with water to form calcium hydroxide ($Ca(OH)_2$) and magnesium hydroxide ($Mg(OH)_2$). The mixture was then transferred into a laboratory blender to provide vigorous agitation while slowly adding 80 mL of 50% phosphoric acid. Sodium hydroxide was periodically added to maintain the pH at the required level. The mixture thickened with the addition of phosphoric acid as hydroxyapatite formed according to Equation 2. The resultant material was then transferred into a 1 L plastic beaker and left to mature for two days at 45 °C in an oven. After the two days, the temperature was raised to 70 °C to dry the material. The obtained apatitic material was subsequently sintered in a furnace at 500 °C, 600 °C, 700 °C, 800 °C and 900 °C for three hours in the presence of air. The ramp rate to peak temperatures was set at 10 °C/min. After sintering, the furnace was turned off to allow the material to cool naturally to room temperature.

Materials characterization

X-ray fluorescence analyses, using energy dispersive X-ray fluorescence (EDXRF) X-ray tube excitation spectrometer (SPECTRO XEPOS) were carried out to determine the elemental compositions of the precursor materials (carbonate rocks). The sample was ground in agate ball mill and sieved through a nylon sieve of 60 μm size. The powder was then mixed with starch (a binder) in a proportion of 1:1 by weight, and homogenized using Retsch mixer mill (20 rev/min, using agate balls) and pressed into pellets in a hydraulic press.

The carbon contents of the carbonate rock materials were determined using CHNS-O analyzer; Thermo Scientific™ FLASH 2000 CHNS-O with thermal conductivity detector (TCD). Helium gas was used as a carrier gas. Exactly 0.21 mg, 0.32 mg and 0.45 mg were weighed into tin cups and loaded on the CHNS-O instrument. The average carbon content of the three samples was reported. Reagent grade BBOT (2,5-(bis(5-tert-butyl-2-benzo-oxazol-2-yl) thiophene) was used as a standard. An empty tin cup was used as a blank sample.

Fourier transform infrared spectroscopy (FTIR) measurements were performed using Bruker Optic GmbH (alpha model, Laser class 1) spectrometer with attenuated total reflectance (ATR). The technique was used for the identification of the major minerals in the carbonate rocks and the chemical characterization of the synthesized apatite material. Tests were conducted in transmittance mode in spectral range 4000–400 cm^{-1} with a resolution of 2 cm^{-1}.

Results and Discussion

Rock material characterization

Elemental analysis

Table 1 presents the X-ray fluorescence analysis results of the white rock materials used in this study. It can be seen from the table that the materials contained magnesium and calcium as the major cations. CHNS-O Analyzer results showed that the carbon contents of the rock materials were 12.4 ± 1%. The high carbon content in the presence of magnesium and calcium as the only major cations is an indication of the high purity of the carbonate rocks.

Table 1: Elemental composition of dolostone

Component (symbol, name)		Average %	Standard deviation
L.O.I.	Loss on Ignition	62.20	0.2
Mg	Magnesium	11.8	0.1
Si	Silicon	0.93	0.01
P	Phosphorus	0.013	0.001
Ca	Calcium	24.92	0.08
Fe	Iron	0.044	0.001

Carbonate rock mineralogical analysis by Fourier transform infrared spectroscopy (FTIR)

Figure 1 presents the FTIR spectrum of the carbonate rock materials used in this study. The rock materials exhibited peaks typical of carbonate materials containing some quartz or silica impurities. The band at around 1200–900 cm^{-1}, ascribable to Si-O and Si-O-Si vibrations (Madejová 2003, Sağın et al. 2012, Sdiri et al. 2010), evidences the presence of quartz/silica.

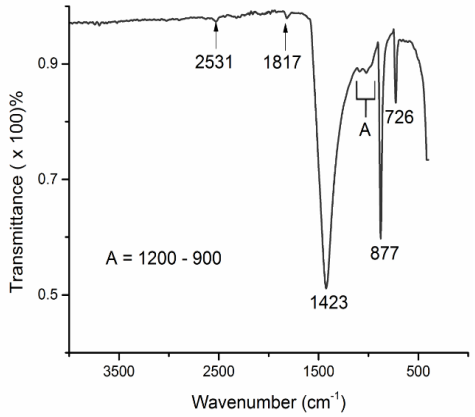

Figure 1: FTIR spectrum of dolostone used in this study.

Several researchers have studied and employed FTIR analysis as a rapid technique for identifying dolomite (Boggs Jr and Boggs 2009, Jovanovski et al. 2002, Stanienda-Pilecki 2019). In this study, FTIR peak positions were used to identify the carbonate rock materials used. The principle behind this carbonate mineral identification technique is that peaks shift from their respective positions because of changes in the chemical environment of the carbonate ion. Variations in the CO_3^{2-} peak locations on the FTIR spectrum show differences in the chemical environment of the ion. The CO_3^{2-} ion chemical environment, due to neighboruring atoms in the lattice crystal structure, varies with the carbonate mineral type, leading to a shift in its peak position on the FTIR spectrum (Pokrovsky et al. 2000, Stanienda-Pilecki 2019, Stanienda 2016).

Literature establishes that free CO_3^{2-} ions exhibit four intra-molecular vibrations: ν_1 (symmetrical stretching), ν_2 (bending beyond the plane), ν_3 (asymmetrical stretching), and ν_4 (bending in the plane) (Pokrovsky et al. 2000, Frost et al. 2008, Boggs Jr and Boggs 2009, Stanienda-Pilecki 2019). When the ion (CO_3^{2-}) is in the crystalline lattice of trigonal anhydrous carbonate minerals, vibrations of

the CO_3^{2-} ion give absorption bands slightly shifted compared to the free ion vibrations (Frost et al. 2008). Of all the carbonate bands (ν_1 - ν_4), the band ν_4 proves to be particularly useful for identification of carbonate minerals (Stanienda-Pilecki 2019). This is because the shift of this band, as the cation changes, is more evident and pronounced (Stanienda 2016, Stanienda-Pilecki 2019).

In this study, the carbonate minerals that make up the rock materials were identified on the bases of the position of $\nu_1 + \nu_4$ and ν_4 bands on the FTIR spectrum. Table 2 presents the peaks (ν_1 - ν_4). The ν_2, ν_3, $\nu_1 + \nu_3$ and those obtained from the literature are also included in Table 2 for comparisons.

Table 2: Selected FTIR bands for carbonate minerals of the materials used in this study (sample peaks) and those obtained from the literature (Gunasecaran et al. 2006, Boggs Jr and Boggs 2009, Stanienda 2016, Stanienda-Pilecki 2019)

Peak type	Sample peaks (This study)	Peaks from literature				
		Dolomite $CaMg(CO_3)_2$	Calcite $CaCO_3$	High Mg-calcite $(Ca_{1-n}Mg_n\ (CO_3)_2$	Magnesite $MgCO_3$	Huntite $CaMg_3(CO_3)_4$
ν_4	726	727–731	712	719	747–748	742–744
ν_2	877	878–883	873–875	876	884–885	869–890
ν_1	1090	1092–1100	1087	1084–1088	1108–1113	1110–1113
ν_3	1424	1431–1451	1409–1415	1426–1437	1448–1456	1530
$\nu_1 + \nu_4$	1817	1815–1822	1797–1799	1800	1827–1831	1825–1828
$\nu_1 + \nu_3$	2531	2525–2538	2512–1519	2517–1519	2535–1537	2581–1583

The $\nu_1 + \nu_4$ and ν_4 band values of the rock materials used in this study (1817 cm^{-1} and 726 cm^{-1}, respectively) generally fall within the range of the diagnostic positions for stoichiometric dolomite (Boggs Jr and Boggs 2009, Stanienda 2016, Stanienda-Pilecki 2019). The appearance of the ν_4 peak at 726 cm^{-1}, which is only 1 cm^{-1} below the literature lower limit for stoichiometric dolomite (727–731 cm^{-1}), may suggest that the mineral deviates slightly from its perfect stoichiometry forming near-stoichiometric dolomite. As can be seen from Table 2, the $\nu_1 + \nu_4$ and ν_4 peaks of the rock materials used in this study are by far located at higher wavenumber values than the values for calcite (Gunasecaran et al. 2006, Stanienda 2016, Stanienda-Pilecki 2019) and high magnesium calcite (Stanienda 2016, Stanienda-Pilecki 2019) reported in the literature (Table 2). This indicates that the material does not contain significant amounts of the minerals.

As can be seen from Figure 1, there were no distinct FTIR peaks at the huntite ($Mg_3Ca(CO_3)_4$) and magnesite ($MgCO_3$) diagnostic wavenumber positions (Stanienda 2016, Stanienda-Pilecki 2019) (Table 2). The wavenumber values of the carbonate materials used in this study are by far closer to the literature values of dolomite than huntite and magnesite. This indicates that the material did not contain a significant amount of the huntite and magnesite minerals.

Hydroxylapatite fourier transform infrared spectroscopy (FTIR) analysis

Literature shows that FTIR spectroscopy is a powerful and comparatively quick technique for chemical analysis of calcium phosphate products (Berzina-Cimdina and Borodajenko 2012). The locations, intensities, width and shapes of the bands on spectrograms provide useful information about the chemical and phase compositions of a calcium phosphate systems (Antonakos et al. 2007, Berzina-Cimdina and Borodajenko 2012, Kabir et al. 2012). FTIR is also a very sensitive technique for determining phase composition (Berzina-

Cimdina and Borodajenko 2012, Kabir et al. 2012).

Figures 2 (a) and (b) show the spectra of the synthesized material sintered at various temperatures. Table 3 presents selected FTIR bands/peaks for synthesized materials sintered at the specified temperatures.

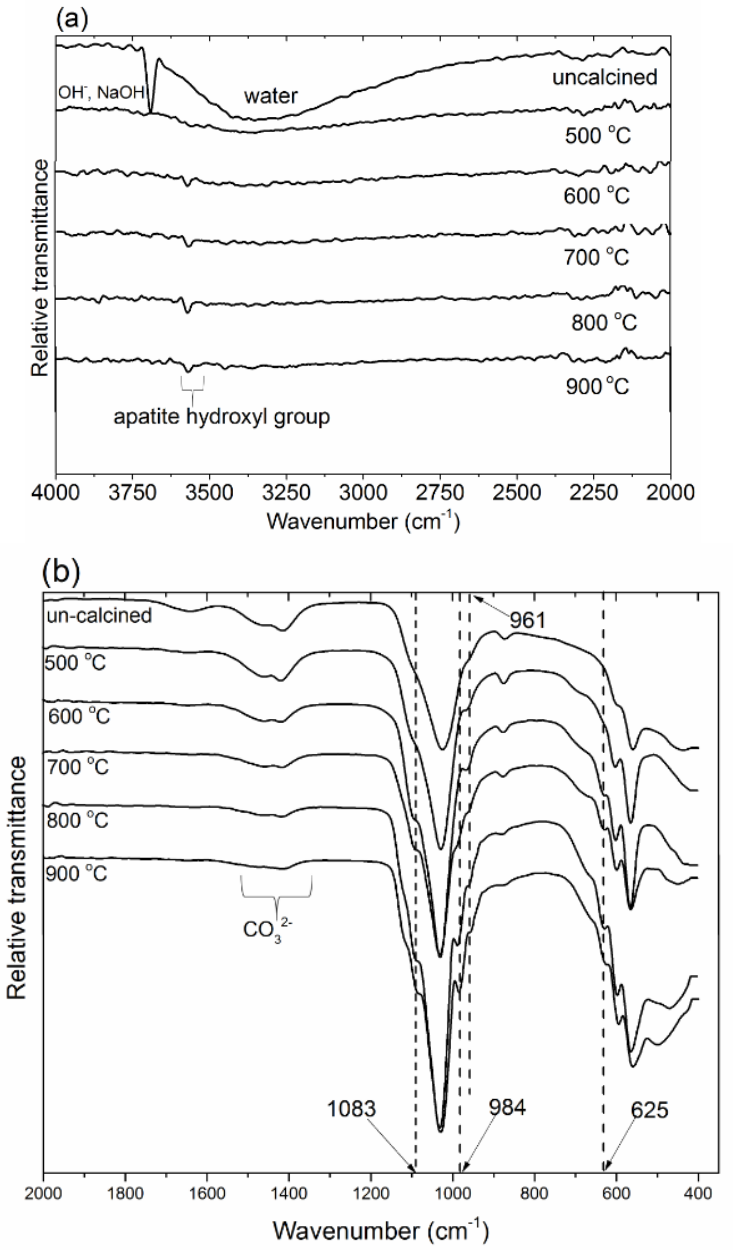

Figure 2: FTIR spectra of the dolostone-derived hydroxylapatite calcined at the annotated temperatures (a) 4000–2000 cm^{-1} (b) 2000–4000 cm^{-1}.

Table 3: Selected FTIR peaks (in cm^{-1}) for the unsintered and sintered dolostone-derived hydroxylapatite sintered at the specified temperatures

Un-sintered	500 °C	600 °C	700 °C	800 °C	900 °C	Assignments
559	562.1	563.6	562.2	560.7	565.19	PO_4^{3-} bending (v_4) (Drouet 2013)
594	600.4	599	596.1	594.7	594.7	PO_4^{3-} bending (v_4) (Kabir et al. 2012)
-	-	625.1	625.6	625.6	625.9	librational OH^- (Drouet 2013)
872.3	873.7	873.7	875.1	875.1	877.9	CO_3^{2-}, HPO_4^{2-} (Drouet 2013)
-	968.6	965.7	962.9	962.9	961.5	PO_4^{3-} stretching (v_1) (Drouet 2013)
-	-	-	-	985.5	984.1	β-Trcalcium phosphate (β-TCP)
1023.8	1026.6	1028.1	1029.4	1028.7	1029.4	PO_4^{3-} bending (v_3) (Kabir et al. 2012)
-	-	-	1083.3	1083.3	1081.8	PO_4^{3-}, (v_3) (Berzina-Cimdina and Borodajenko 2012)
1418.8	1416	1418.8	1414.6	1416.6	1417.4	CO_3^{2-} group (Drouet 2013, Kabir et al. 2012)
1459.9	1458.5	1457.1	1458.5	1457.7	1475.1	CO_3^{2-} group (Drouet 2013, Kabir et al. 2012)
-	-	3569.8	3569.8	3572.1	3572.4	Apatite OH^- (Drouet 2013)
3691.6	-	-	-	-	-	$Mg(OH)_2/Ca(OH)_2$
3353	-	-	-	-	-	water absorbed (Berzina-Cimdina and Borodajenko 2012)

As can be seen from Figure 2 (a), the FTIR spectrum of the synthesized un-sintered apatite features a narrow and sharp peak at 3692 cm^{-1}. This band was assigned to non-apatitic OH^- ion of sodium hydroxide (NaOH). The band (assignable to OH^- of NaOH) disappeared from the spectra of the synthesized material upon sintering at 500 °C. To ascertain the assignment of the band and distinguish it from the neighbouring peaks observable upon sintering the material, two experiments were conducted: (1) soaked calcined dolostone powder (the precursor) in sodium hydroxide solution, dried it and calcined a portion of it. The un-calcined portion was labelled portion "A" while the calcined one was called portion "B", (2) synthesized Mg-hydroxylapatite in excess of the heat pre-treated dolostone powder where the same procedure described in the "Materials and Methods" section was used except that phosphoric acid was reduced by 25%. The un-calcined portion was labelled C and the calcined D.

Figure 3 presents the spectra obtained in experiments 1 and 2. The un-calcined material labelled A in experiment 1 (heat pretreated dolostone powder soaked in NaOH and dried) exhibited the peak, though shifted from 3692 cm^{-1} to 3686 cm^{-1} (Figure 3, spectrum A). The sample material labelled B (heat pre-treated dolostone powder soaked in NaOH solution and calcined) did not exhibit the band but featured a new peak assignable to MgO/CaO at 3642 cm^{-1} (Figure 3, spectrum B). This shows that the peak for NaOH [and $Ca(OH)2/Mg(OH)_2$] is lost upon sintering at a temperature below 500 °C. The sample material labelled C (synthesized in experiment 2 using 25% less phosphoric acid,

that is, in excess CaO/MgO) also exhibited the sharp peak at 3691 cm^{-1} (Figure 3 C). It is worth noting that, despite the presence of three OH containing species [NaOH, $Ca(OH)_2$ and $Mg(OH)_2$], the spectra of sample A and C showed only one OH band. The sample material labelled D (synthesized in experiment 2 and calcined at 800 °C) did not show the band (at ~3686– 3692 cm^{-1}) but exhibited bands at 628 cm^{-1} and 3672 cm^{-1}, assignable to apatitic hydroxyl groups, and another one at 3642 cm^{-1}(Figure 3, spectrum D). The absence of a band at ~3686–3692 cm^{-1} (observable in sample A and C) from the spectrum of sample D confirms the disappearance of the hydroxide band in the calcium/magnesium phosphate matrix. Since the band at 3642 cm^{-1} was also observed on the spectrum of sample material labelled B (the heat pre-treated dolomite powder soaked in NaOH solution and calcined, in experiment 1), it is confirmed that the band originates from CaO/MgO. The band at 3572 cm^{-1} on the spectrum of sample D signifies the position of the apatitic hydroxyl group in this material. The results of the two experiments warrant authority to conclude that: (1) the peak at ~3692-3686 cm^{-1} may originate from the OH^- of either NaOH or $Ca(OH)_2$ /$Mg(OH)_2$, (2) the peak for apatitic hydroxyl group in this material (carbonated magnesium-substituted hydroxylapatite) features at around 3572 cm^{-1}, (3) the peaks for MgO/CaO is observable at around 3642 cm^{-1}.

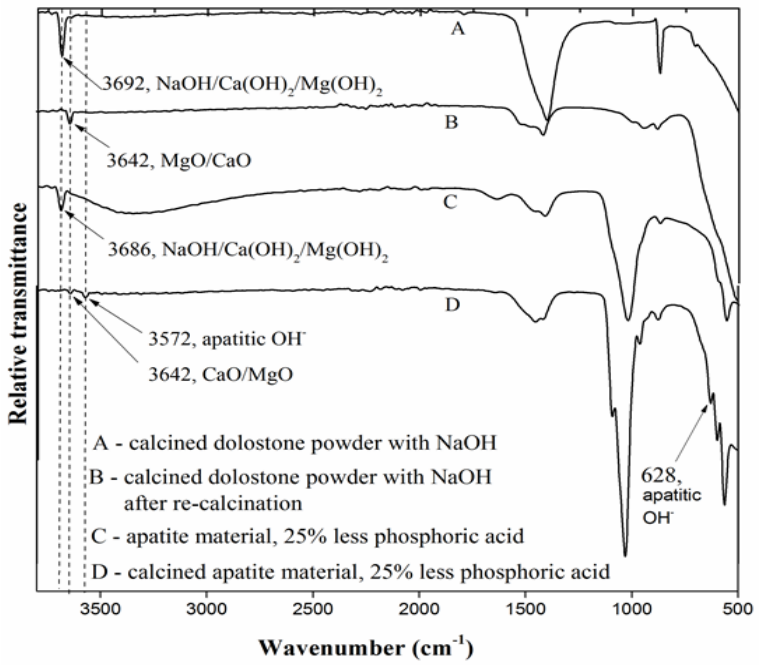

Figure 3: Spectra of various materials showing peaks for NaOH/ $Mg(OH)_2$ $Ca(OH)_2$, MgO/CaO and apatititic OH^-. A is calcined dolostone powder with sodium hydroxide, B is calcined dolostone powder with sodium hydroxide after re-calcination, C is apatite mineral synthesized using 60 mL (25% less) of phosphoric acid, D calcined apatite material synthesized using 60 mL E calcined apatite material synthesized using 80 mL of phosphoric acid.

The dolostone derived hydroxylapatite synthesized in this study (whose data is presented in Figure 2 (a) and (b), and Table 3) exhibited peaks at 1418 cm^{-1} and 1460 cm^{-1} (Figure 2(b). The peaks indicate the presence of carbonate ion (CO_3^{2-}). It is traditionally accepted that the bands at ~1545, 1450~1457, and ~880 cm^{-1} indicate type-A substitution (replacement of OH^- by CO_3^{2-} in the HA structure), while the bands at ~1465, ~1413, and ~873 cm^{-1} signify type-B substitution (replacement of OH^- by CO_3^{2}). Ren and Leng (2012), however, asserted that the bands at ~880 cm^{-1}, ~1413 cm^{-1}, and~1450 cm^{-1} should not be used to identify carbonated apatite as they may result from carbonate absorption on surfaces of apatite crystals or separate carbonate phases present with apatite crystals. It was suggested that infrared (IR) characteristic bands of carbonate substitution in apatites should be ν_3 band at ~1546 cm^{-1} for type-A and ν_3 band~1465 cm^{-1} for type-B.

In the current study, there was no peak observed at ~1546 cm^{-1} which, according to Ren and Leng (2012), suggests the absence of type-A substitution. The band which, according to Ren and Leng (2012), should appear at ~1465 cm^{-1} in type-B substitution featured at ~1460 cm^{-1}. The featuring of the band at 1460 cm^{-1} in the absence of the type-A diagnostic peak at around 1546 cm^{-1} suggests domination of type-B substitution.

At temperatures above 600 °C, two apatite OH^- diagnostic bands emerged, one with a peak at 3570 cm^{-1} (stretching mode) and the other at 625 cm^{-1} (librational mode). Both the stretching and the librational peaks slighly shifted to higher wavenumber values as sintering temperature increased (Table 3). The peak for the stretching mode of the apatitic hydroxyl is shown in Figure 2 (b), while the librational peak is shown in Figure 2 (b). The broken verticle lines have been introduced in Figure 2 (b) including at 625 cm^{-1} to increase the visibility of bands. The two hydroxylapatite diagnostic peaks were not observed on the spectra of the un-sintered materials, and the materials sintered at 500 °C (Figure 2 (a) and (b)). The absence of these peaks from the spectra of the materials sintered at low temperatures could be caused by the following inter-related phenomena: (1) low degree of crystallinity, (2) substitution (magnesium and carbonate being the major substitutions) and (3) non-stoichiometry of the hydroxylapatite (Antonakos et al. 2007, Berzina-Cimdina and Borodajenko 2012, Drouet 2013, Prekajski et al. 2016).

Low degree of crystallinity tends to enlarge vibrational bands, covering or masking weak signals (Antonakos et al. 2007, Drouet 2013, Prekajski et al. 2016). Generally, this is a characteristic of hydroxylapatite synthesized by aqueous precipitation due to being composed of nano-metric particles (Drouet 2013). The effect is known to be more profound when the hydroxylapatite contains Mg^{2+} in its structure which inhibits the apatite crystallization and reduces crystallite size (Bertoni et al. 1998, Bigi et al. 1993). Since the precursor material used in this study (dolostone) contains Mg and Ca as the major cations, the synthesized hydroxylapatite should be magnesium and carbonate substituted.

Non-stoichiometry and substitution, on the other hand, disfavour the presence of OH^- ions in apatite channels (Antonakos et al. 2007, Drouet 2013, Prekajski et al. 2016). The substitution of Ca^{2+} and PO_4^{3-} by species such as Mg^{2+} and CO_3^{2-} (type-B carbonate substitution), respectively is known to induce vacancies at the OH^- sites leading to low concentrations of OH^- in the lattice structure of hydroxylapatite, and hence the diminished OH^- diagnostic peaks on the FTIR spectrum (Antonakos et al. 2007, Drouet 2013, Prekajski et al. 2016). The hydroxyl (OH^-) ions themselves may also be replaced by carbonate ions (CO_3^{2-}) (type-A carbonate substitution). Fleet and Liu (2007) observed that increasing carbonate content resulted in a progressive reduction in intensity, and eventually total disappearance, of the OH^-

stretch and librational bands at 3570 cm^{-1} and 631 cm^{-1}, respectively.

The featuring of the apatite OH^- band on the FTIR spectra of materials sintered at elevated temperatures, but not on that of the un-sintered materials and materials sintered at low temperatures evidences increase in crystallinity as calcination temperature increases (Figure 2 (a) and (b)).

A progressive shift of the main v_3 PO_4^{3-} peak to lower energy with increase in sintering temperature (1023.8 cm^{-1} to 1029.4 cm^{-1}) was observed (Table 2). The shift indicates that the P–O bond length becomes longer as the carbonate group is thermally driven off the apatite structure during calcination. Phase transformation of the material, as calcination temperature increases, is testified by the emergence of a peak at ~985 cm^{-1} upon sintering at 700 °C. As Figure 2 (b) depicts, the band starts as a perceptible peak at 700 °C and becomes more distinct and prominent at 800 °C (the vertical broken line that touches wavenumber axis at ~984 cm^{-1} will help to locate the band). The peak is assignable to beta-tricalcium phosphate (magnesium-substituted beta-tricalcium phosphate, or Mg-substituted β-TCP, or β-$Ca_{3-x}Mg_x(PO_4)_2$). The appearance of this peak indicates the conversion of the magnesium substituted-hydroxylapatite (Mg-HA) into Mg-substituted β-TCP. Literature shows that hydroxylapatite begins to convert into beta-tricalcium phosphate (β-TCP) at higher temperatures, above 1000 °C (Bertoni et al. 1998). The lowering of the conversion temperature observed in this work could have been caused by the presence of Mg^{2+} in the apatite lattice structure. Literature shows that Mg^{2+} destabilizes the apatitic structure, favouring its thermal conversion into beta-tricalcium phosphate (β-$Ca_3(PO_4)_2$, β-TCP) (Bertoni et al. 1998).

There were no peaks on the FTIR spectra associated with other calcium phosphate phases such as brushite (dicalcium phosphate dihydrate $CaHPO_4.2H_2O$; DCPD)), octacalcium phosphate ($Ca_8H_2(PO_4)_6.5H_2O$, OCP, at ~930 cm^{-1}) or pyrophosphates ($P_2O_7^{4-}$, at ~720 cm^{-1}).

The results show that magnesium-substituted hydroxylapatite (Mg-HA) can be synthesized using dolostone as a source of calcium and magnesium. The synthesized Mg-HA begun to convert to Mg-substituted β-TCP (β-$Ca_{3-x}Mg_x(PO_4)_2$) at 600–700 °C, forming a biphasic apatitic material.

Conclusion

A carbonated magnesium–substituted hydroxylapatite (Mg-HA) was synthesized from heat pre-treated dolostone with near-stoichiometric dolomite. The synthesized apatite exhibited a low degree of crystallinity, possibly due to magnesium substitution and nano-metric crystallite size. Sintering the apatite resulted in improving crystallinity and the formation of magnesium-substituted beta tri-calcium phosphate (Mg-substituted β-TCP, β-$Ca_{3-x}Mg_x(PO_4)_2$) phase. The conversion temperature of the hydroxylapatite (magnesium and carbonate substituted) to Mg-substituted β-TCP was found to be lower than its unsubstituted counterparts reported in literature. Our future work will focus on assessing the materials' performance and applicability in water decontamination (with emphasis on fluoride and heavy metal removal) and disinfection (removal of pathogenic microbes).

Acknowledgement

This work was funded by the African Development Bank (AfDB) with grant number 2100155032816.

Declaration of Interest

The authors declare that there is no conflict of interest whatsoever on this research work.

References

Alioui H, Bouras O and Bollinger JC 2019 Toward an efficient antibacterial agent: Zn-and Mg-doped hydroxyapatite nanopowders. *J. Environ. Sci. Health A* 54(4): 315-327.

Antonakos A, Liarokapis E and Leventouri T 2007 Micro-Raman and FTIR studies of synthetic and natural apatites. *Biomaterials* 28(19): 3043-3054.

Avram A, Frentiu T, Horovitz O, Mocanu A, Goga F and Tomoaia-Cotisel M 2017 Hydroxyapatite for removal of heavy metals from wastewater. *Studia UBB Chemia.* 4: 93-104.

Bertoni E, Bigi A, Cojazzi G, Gandolfi M, Panzavolta S and Roveri N 1998 Nanocrystals of magnesium and fluoride substituted hydroxyapatite. *J. Inorg. Biochem.* 72(1-2): 29-35.

Berzina-Cimdina L and Borodajenko N 2012 Research of calcium phosphates using Fourier transform infrared spectroscopy. In: Theophile J (Ed.) *Infrared Spectroscopy-Materials Science, Engineering and Technology* vol. 12 (pp. 251-263), InTechOpen, London.

Bigi A, Falini G, Foresti E, Ripamonti A, Gazzano M and Roveri N 1993 Magnesium influence on hydroxyapatite crystallization. *J. Inorg. Biochem.* 49(1): 69-78.

Boggs Jr and Boggs S 2009 Petrology of Sedimentary Rocks, 2nd ed, Cambridge University Press.

Demishtein K, Reifen R and Shemesh M 2019 Antimicrobial properties of magnesium open opportunities to develop healthier food. *Nutrients* 11(10): 2363.

Drouet C 2013 Apatite formation: why it may not work as planned, and how to conclusively identify apatite compounds. *Biomed Res. Int.* 2013: 1-12.

Fleet ME and Liu X 2007 Coupled substitution of type A and B carbonate in sodium-bearing apatite. *Biomaterials* 28(6): 916-926.

Frost RL, Martens WN, Wain DL and Hales MC 2008 Infrared and infrared emission spectroscopy of the zinc carbonate mineral smithsonite. *Spectrochim. Acta A.* 70(5): 1120-1126.

Jamarun N, Azharman Z, Arief S, Sari TP, Asril A and Elfina S 2015 Effect of temperature on synthesis of hydroxyapatite from limestone. *Rasayan J. Chem.* 8(1): 133-137.

Jovanovski G, Stefov V, Šoptrajanov B and Boev B 2002 Minerals from Macedonia. IV. Discrimination between some carbonate minerals by FTIR spectroscopy. *J. Mineral. Geochem.* 177(3): 241-253.

Kabir S, Ahmed S, Mustafa A, Ahsan M and Islam S 2012 Synthesis and characterization of Fe-doped hydroxyapatite. *Bangladesh J. Scient Ind. Res.* 47(1): 1-8.

Klinkaewnarong J and Utara S 2018 Ultrasonic-assisted conversion of limestone into needle-like hydroxyapatite nanoparticles. *Ultrason Sonochem.* 46: 18-25.

Kolmas J, Groszyk E and Kwiatkowska-Różycka D 2014 Substituted hydroxyapatites with antibacterial properties. *Biomed Res. Int.* 2014.

Madejová J 2003 FTIR techniques in clay mineral studies. *Vib. Spectrosc.* 31(1): 1-10.

Mousa SM, Ammar NS and Ibrahim HA 2016 Removal of lead ions using hydroxyapatite nano-material prepared from phosphogypsum waste. *J. Saudi Chem. Soc.* 20(3): 357-365.

Narasaraju T and Phebe D 1996 Some physico-chemical aspects of hydroxylapatite. *J. Mater. Sci.* 31(1): 1-21.

Pokrovsky O, Mielczarski J, Barres O and Schott J 2000 Surface speciation models of calcite and dolomite/aqueous solution interfaces and their spectroscopic evaluation. *Langmuir* 16(6): 2677-2688.

Predoi D, Iconaru SL, Predoi MV, Stan GE and Buton N 2019 Synthesis, characterization, and antimicrobial activity of magnesium-doped hydroxyapatite suspensions. *Nanomaterials* 9(9): 1295.

Prekajski M, Mirković M, Todorović B, Matković A, Marinović-Cincović M, Luković J and Matović B 2016 Ouzo

effect–new simple nanoemulsion method for synthesis of strontium hydroxyapatite nanospheres. *J. Eur. Ceram. Soc.* 36(5): 1293-1298.

Ren FZ and Leng Y 2012 Carbonated apatite, type-A or type-B? In *Key Eng. Mater. Vol.* 493: pp. 293-297, Trans Tech Publications Ltd.

Sağın EU, Böke H, Aras N and Yalçın Ş 2012 Determination of $CaCO_3$ and SiO_2 content in the binders of historic lime mortars. *Mater Struct.* 45(6): 841-849.

Sdiri A, Higashi T, Hatta T, Jamoussi F and Tase N 2010 Mineralogical and spectroscopic characterization, and potential environmental use of limestone from the Abiod formation, Tunisia. *Environ. Earth Sci*. 61(6): 1275-1287.

Stanienda KJ 2016 Carbonate phases rich in magnesium in the Triassic limestones of the eastern part of the Germanic Basin. *Carbonates Evaporites* 31(4): 387-405.

Stanienda-Pilecki KJ 2019 The importance of fourier transform infrared spectroscopy in the identification of carbonate phases differentiated in magnesium content. *Spectroscopy* 34(6): 32-42.

Suphatchaya L, Manlika P, Chutima J, Nopakarn C, Kriangkrai T, Gobwute R, Phuwadol B and Chamnan R 2019 Synthesis of hydroxyapatite with antibacterial properties using a microwave-assisted combustion method. *Scientific Reports* 9(1).

Sternitzke V, Kaegi R., Audinot JN, Lewin E, Hering JG and Johnson CA 2012 Uptake of fluoride from aqueous solution on nano-sized hydroxyapatite: examination of a fluoridated surface layer. *Environ. Sci. Technol*. 46(2): 802-809.

Wagutu AW, Machunda R and Jande YAC 2018 Crustacean derived calcium phosphate systems: Application in defluoridation of drinking water in East African rift valley. *J. Hazard. Mater*. 347: 95-105.

Xu Y, Wang D, Yang L and Tang H 2001 Hydrothermal conversion of coral into hydroxyapatite. *Mater. Charact.* 47(2): 83-87.